Water Science & Technology

IWA PUBLISHING

Water Science & Technology Vol 84 No 5, 1146 doi: 10.2166/wst.2021.286

Ultrasound assisted Fenton-like degradation of dyes using copper doped graphitic carbon nitride

Chongqing Wang[a,*], Rong Huang[a], Ruirui Sun[a] and Hui Wang[b]

[a] School of Chemical Engineering, Zhengzhou University, Zhengzhou 450001, China
[b] School of Chemistry and Chemical Engineering, Central South University, Changsha 410083, China
*Corresponding author. E-mail: zilangwang@126.com

ABSTRACT

A novel copper doped graphitic carbon nitride (Cu-C_3N_4) was successfully synthesized and used as an effective Fenton-like catalyst. Cu-C_3N_4 was characterized by scanning electron microscopy, surface area analyzer, Fourier transform infrared spectroscopy, X-ray diffractometer, and X-ray photoelectron spectroscopy. Effect of process parameters including catalyst dosage, hydrogen peroxide (H_2O_2) concentration, solution pH, and initial methylene blue (MB) concentration was investigated to evaluate catalytic performance. The pseudo first-order kinetic model was used to describe the catalytic process. The enhancement of MB degradation is observed assisted by ultrasound. MB degradation of 96% is obtained within 30 min in Cu-C_3N_4/H_2O_2/ultrasound system, and the corresponding rate constant is 0.099 min^{-1}. Effective MB degradation is obtained over a broad pH range (3.3–9.9). The catalytic mechanism is examined by ultraviolet-visible spectra, quenching test, and electron spin resonance determination. The dominant mechanism of MB degradation is ascribed to the ultrasonic H_2O_2 activation by Cu-C_3N_4 for hydroxyl radical generation. Cu-C_3N_4 has good reusability and is effective to degrade rhodamine B and acid orange 7. This work not only contributes to the field of wastewater treatment, but also provides insights into the synthesis of Fenton-like catalysts. The results manifest that Cu-C_3N_4 is a promising Fenton-like catalyst for dye degradation in the field of environmental pollution remediation.

Key words: copper doping, dye degradation, Fenton-like reaction, graphitic carbon nitride, hydroxyl radical

HIGHLIGHTS

- A novel Cu doped g-C_3N_4 is easily synthesized.
- Cu species uniformly doped on porous g-C_3N_4 contribute to catalytic ability.
- Ultrasound significantly improves MB degradation in the presence of Cu-C_3N_4/H_2O_2.
- MB degradation is effectively obtained in a broad pH range.
- Plausible mechanism of H_2O_2 activation for •OH generation is revealed for MB degradation.

GRAPHICAL ABSTRACT

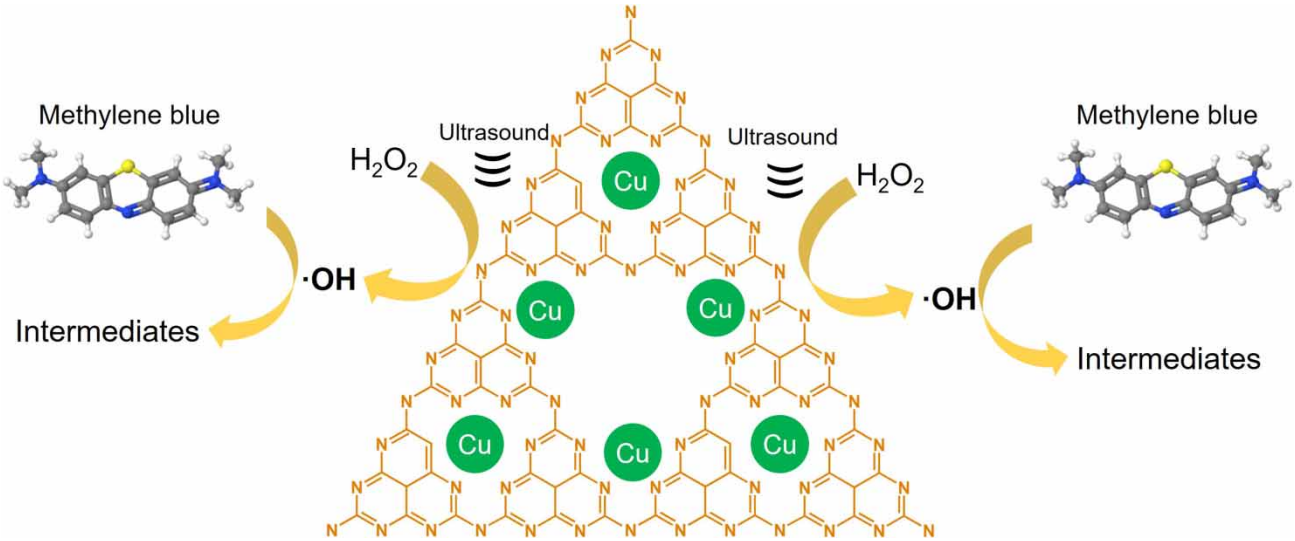

INTRODUCTION

With rapid industrial development, large amounts of persistent organic pollutants are discharged into the natural environment and cause serious environmental pollution. Approximately 80% of total global wastewater is released into the environment. The wastewater emission poses serious threats to ecosystem and public health (Mian & Liu 2018). Wastewater pollution has been a global challenge in the field of environmental remediation. Dyes are common organic pollutants in wastewater from textile, printing, leather tanning, and cosmetic industries, and they are toxic to ecosystems and the human body (Chanikya *et al.* 2021). There is special concern about removal of toxic dyes from wastewater, which is still challenging (Routoula & Patwardhan 2020).

Conventional techniques, such as chemical coagulation, adsorption, and biological oxidation, generally cause unsatisfactory results for wastewater treatment (Kothai *et al.* 2021). Advanced oxidation processes based on reactive radicals are promising for removing toxic dyes from wastewater due to high oxidizability, complete mineralization, and easy operation. The Fenton reaction is an effective way to generate hydroxyl radicals (•OH) with high oxidation ability (E = 2.80 V/NHE). Fenton processes are widely applied to wastewater treatment for removing organic pollutants. However, homogeneous Fenton processes suffer from the shortcomings of narrow pH range, producing large amounts of iron sludge, and impractical catalyst recovery (Ma *et al.* 2017). Iron-based Fenton catalysts confront the problem of narrow operation pH (Wang *et al.* 2021a). In this regard, extensive efforts have been conducted to develop effective Fenton-like catalysts operated over a wide pH range (Xin *et al.* 2021). Because of high abundance, low cost, and the striking reactivity towards hydrogen peroxide (H_2O_2), copper-based catalysts have received increasing global attention (Gawande *et al.* 2016). Copper ions are more efficient than iron ions for H_2O_2 activation to generate radical species. As shown in Equations (1)–(4), the rate constant of copper ions towards H_2O_2 is much higher than that of iron ions (Zhang *et al.* 2017; Wang *et al.* 2021a). In addition, H_2O_2 activation by cupric ion occurs over a broad pH range, which is highly attractive for the oxidation of organic pollutants in neutral conditions (Bokare & Choi 2014). Copper-based catalysts, such as copper/carbon composites (Wang *et al.* 2019a) and nanoscale zero-valent copper (Shah *et al.* 2020), have been investigated for Fenton-like degradation of organic pollutants in wastewater. Considering catalytic activity, synthesis process, and catalyst reusability, there is still big research gap for developing effective Fenton-like catalysts:

$$Fe^{2+} + H_2O_2 \rightarrow Fe^{3+} + \bullet OH + HO^- \; k = 76\,M^{-1}s^{-1} \quad (1)$$

$$Fe^{3+} + H_2O_2 \rightarrow Fe^{2+} + \bullet OOH + H^+ \; k = 0.001 - 0.02\,M^{-1}s^{-1} \quad (2)$$

$$Cu^{+} + H_2O_2 \rightarrow Cu^{2+} + \bullet OH + HO^- \; k = 10000\,M^{-1}s^{-1} \quad (3)$$

$$Cu^{2+} + H_2O_2 \rightarrow Cu^{+} + \bullet OOH + H^+ \; k = 460\,M^{-1}s^{-1} \quad (4)$$

The synthesis of nanoscale catalysts is an attractive strategy for improving catalytic activity. Metals supported on carbon matrix such as activated carbon, biochar, and graphene have been reported (Wu *et al.* 2020; Wang *et al.* 2021b). Graphitic carbon nitride (g-C_3N_4), a layered material with a 2D π-conjugated polymeric structure, is a promising matrix for loading active metals. The unique physical structure, excellent chemical stability and tunable electronic properties support the photocatalytic activity in environmental applications (Yang *et al.* 2020; Hasija *et al.* 2021). g-C_3N_4 can be easily synthesized through the thermal polymerization of low-cost N-rich precursors such as urea, melamine, dicyandiamide, and thiourea (Jourshabani *et al.* 2020; Nguyen *et al.* 2021). Various modification strategies, such as elemental doping, heterojunction, defects engineering and structural regulation, have been reported to improve the properties for potential applications (Chen *et al.* 2020a). Due to the chemical stability and ligand-field effects, metal doped g-C_3N_4 can be promising candidates for Fenton-like catalysts (Zhu *et al.* 2019).

To solve the problem of developing effective Fenton-like catalysts, a novel copper doped g-C_3N_4 was designed and facilely synthesized. Methylene blue (MB) was chosen as a target pollutant. Ultrasound-assisted MB degradation was evaluated in the presence of H_2O_2. The objectives of this study are (1) to characterize the catalyst, (2) to determine the catalytic performance, and (3) to discuss the plausible catalytic mechanism.

METHODS

Materials

All used chemicals were analytically pure, including hydrogen peroxide (H_2O_2; Sinopharm Chemical Reagent Co., Ltd), copper chloride ($CuCl_2{\cdot}2H_2O$; Sinopharm Chemical Reagent Co., Ltd), melamine ($C_3H_6N_6$; Macklin Reagent Co., Ltd), nitric acid (HNO_3; Sinopharm Chemical Reagent Co., Ltd), sodium hydroxide (NaOH; Sinopharm Chemical Reagent Co., Ltd), isopropyl alcohol (IPA; C_3H_8O; ALADDIN Reagent (Shanghai) Co., Ltd), methylene blue ($C_{16}H_{18}ClN_3S$; Tianjin Kemiou Chemicals Co., Ltd), rhodamine B ($C_{28}H_{31}ClN_2O_3$; Tianjin Guangfu Fine Chemical Research Institute), and acid orange 7 ($C_{16}H_{11}N_2NaO_4S$; ALADDIN Reagent (Shanghai) Co., Ltd). Ultrapure water from a Millipore Milli-Q water purification system was used in experiments.

Catalyst synthesis

The synthesis of catalysts was conducted by metal ion blending and carbonization as shown in Fig. S1 (Supporting Information). First, melamine (2 g) and copper chloride (1.62 g) were dissolved in 10 mL methanol to obtain a uniform solution. Methanol was the chosen solvent because both melamine and copper chloride can be dissolved in it. After removing methanol by stirring at 60 °C, the solid product with uniformly mixed melamine and copper was obtained. Finally, the solid product was calcined in a muffle furnace with limited oxygen. The temperature was elevated to 550 °C with a ramping rate of 5 °C/min and maintained at 550 °C for 120 min. The calcined product was rinsed using ethanol solution (50%) to remove residual substances or by-products of carbonization. After drying at 100 °C for 8 h, the obtained copper doped carbon nitride (Cu-C_3N_4) was used as a catalyst.

Characterizations

A scanning electron microscopy (SEM) equipped with energy dispersive X-ray spectroscopy (EDS; FEI Quanta FEG 250) was used to analyze the morphology and surface elements. The N_2 adsorption–desorption isotherm was determined at 77 K to analyze the surface area using a surface area analyzer (Micromeritics, ASAP 2020, USA). Fourier transform infrared spectroscopy (FTIR; Frontier, PerkinElmer, USA) was used to record the FTIR spectrum. X-ray diffractometer (XRD; Ultimate IV, Rigaku Co., Japan) was employed to determine the chemical phases. X-ray photoelectron spectroscopy (XPS; Thermo ESCALAB 250XI, Thermo Scientific, USA) was used to examine the surface elements. An ultraviolet–visible spectrophotometer (UV–vis; UV-2600, Shimadzu, Japan) was employed to measure the absorbance of characteristic peak and UV–vis spectra of dye solution. A JES FA200 spectrometer was used to detect the electron spin resonance (ESR) signals using 5,5-dimethyl-1-pyrroline-N-oxide (DMPO) as the radical-capture reagent.

Catalytic experiments

The research design of this work is schematically shown in Fig. S2. Batch experiments were conducted in 150 mL conical flask at room temperature. The conical flask containing 50 mL MB solution was put in an ultrasonic cleaner (40 kHz, 150 W; XM-3200UVF, Xiaomei Instrument Limited Company, China). Experimental parameters were investigated including catalyst (0–0.6 g/L), H_2O_2 (0–40 mM), pH (3.3–9.9), and MB concentration (10–30 mg/L). Quenching experiments were

conducted using IPA as radical scavenger. The reusability of the catalyst was studied for MB degradation through five cycles. Catalytic degradation of different dyes was also evaluated. During the experiments, a solution sample was taken out, centrifugally separated, and immediately determined using an UV–vis spectrophotometer. The calculation of MB removal is described in Supporting Information. The pseudo first-order model has been widely used for kinetic analysis. Reaction rate was examined by the kinetic model (described in Supporting Information).

RESULTS AND DISCUSSION

Characterizations

The morphology and elemental distribution of Cu-C_3N_4 are characterized by SEM-EDS. The g-C_3N_4 is a layered massive particle (Hu *et al.* 2019a). As shown in Figure 1, Cu-C_3N_4 shows a sheet-like structure similar to that of g-C_3N_4. Aggregated nanosized particles without well-defined morphology were observed, which may be the doped copper oxides. Cu-C_3N_4 also manifests a porous morphology with intersect channels, which resulted from the release of gaseous products in the heating process (Ma *et al.* 2017; Qin *et al.* 2019). Fig. S3 manifests the major elements of Cu, C, N, and O. Elemental mapping displays the uniform distribution of C, N, O, and Cu in the material, confirming that Cu is doped on g-C_3N_4 (Hu *et al.* 2019a).

As shown in Figure 2(a), the N_2 adsorption–desorption isotherm of Cu-C_3N_4 shows a type IV isotherm with an H3 hysteresis loop according to the IUPAC classification, which suggests the slit-shaped pores resulted from aggregated particles (Ma *et al.* 2017; Jiang *et al.* 2019). The surface area and pore parameters are listed in Table S1 (Supporting Information). The BET surface area is 7.18 m^2/g. The pore size distribution plotted by the BJH method displays a bimodal pore distribution ranging from 2 to 10 nm. The average pore diameter is 12 nm.

Figure 2(b) shows the FTIR spectrum of Cu-C_3N_4. The peaks at 3,508–3,423 cm^{-1} are related to the stretching vibration of the N-H bond and -OH bond (Wang *et al.* 2019b). The characteristic peaks in the region ranging from 1,132 to 1,624 cm^{-1} (1,132, 1,292, 1,403, and 1,624 cm^{-1}) corresponded to the trigonal C-N(-C)-C or the bridging C-NH-C units (Yao *et al.* 2015). The peak associated with the breathing vibration of the s-triazine units appears at 781 cm^{-1}, lower that of g-C_3N_4 (at around 807 cm^{-1}) (Muniandy *et al.* 2017). The peak at 549 cm^{-1} may be ascribed to the stretching vibration of the Cu-N bond, implying that copper species are chemically coordinated to g-C_3N_4 (Dong *et al.* 2017).

The crystallinity of Cu-C_3N_4 was examined by XRD analysis (Figure 2(c)). The diffraction peak at 2-theta of 27.7° is ascribed to the (002) plane for graphitic materials (PDF#87-1526), suggesting the presence of g-C_3N_4 structure (Wang *et al.* 2019b). The diffraction peaks at 2-theta of 32.4°, 35.4°, 38.6°, 48.8°, 53.3°, 58.2°, 61.5°, 66.2°, and 67.9°, which are indexed to the (1 1 0), (1 1 −1), (1 1 1), (2 0 −2), (0 2 0), (2 0 2), (1 1 −3), (3 1 −1), and (1 1 3) crystal planes of CuO (PDF#48-1548) (Feng *et al.* 2019). The peaks at 2-theta of 36.4° and 41.2° are associated with the (1 1 1) and (2 0 0) crystal planes of Cu_2O (PDF#65-3288) (Omrani & Nezamzadeh-Ejhieh 2020). The diffraction peaks at 2-theta of 43.2°, 50.4°, and 74.8° are attributed to the (1 1 1), (2 0 0), and (2 2 0) crystal planes of Cu (PDF#65-9026) (Zhang *et al.* 2020a).

The signals of C 1s, N 1s, O 1s, and Cu 2p are observed at around 285 eV, 399 eV, 530 eV, and 932 eV in the XPS spectra of Cu-C_3N_4 (Figure 2(d)). As shown in Figure 2(e), the high-resolution XPS spectra of C 1s manifest the peaks at 284.8 eV (C-C), 286.2 eV (C-O), and 288.3 eV (N-C = N) (Zhang *et al.* 2020b; Song *et al.* 2021). Figure 2(f) displays the high-resolution N 1s spectra. The peaks at 398.9 eV, 399.6 eV and 400.7 eV are assigned to the sp^2-hybridized pyridine nitrogen (C-*N* = C), tertiary pyrrolic nitrogen (N-C_3), and C-N-H groups (Li *et al.* 2018a). High-resolution O 1s spectra show peaks at 529.9 eV and 531.5 eV (Figure 2(g)), which are associated to the oxygen coordinated with copper (Cu-O) and the hydroxyl groups (-OH) (Kumar *et al.* 2014). Figure 2(h) shows the high-resolution XPS spectra of Cu 2p. The binding energy peaks at 932.9 eV and 952.8 eV correspond to Cu^+ or Cu^0 (Song *et al.* 2021). The peaks at 935.1 eV and 954.9 eV are attributed to the presence of Cu^{2+} (Liu & Hensen 2013). The peak at 570.1 eV in the Cu LMM spectrum confirms the presence of Cu^+. In addition, the shakeup satellite peaks are observed at 942.5 eV and 962.5 eV (Liu & Hensen 2013). The peak fittings of high-resolution Cu 2p spectra reveal the existence of Cu^{2+}, Cu^+, and Cu^0 in Cu-C_3N_4, which agrees with XRD analysis. Combining the FTIR, XRD, and XPS analysis, it can be concluded that copper is chemically incorporated into the g-C_3N_4 structure, probably embedded in the cavities of g-C_3N_4, or formed copper porphyrins and phthalocyanines (Dong *et al.* 2017).

Effect of catalyst dosage

It is reported that ultrasound is effective to enhance Fenton-like reactions (Wang *et al.* 2020a). Fig. S4 shows the comparison of MB degradation under ultrasound and oscillation. MB removal increases progressively with increasing time. The removal is approximately 80% at 90 min under oscillation, while it reaches above 90% at 40 min assisted by ultrasound. The pseudo

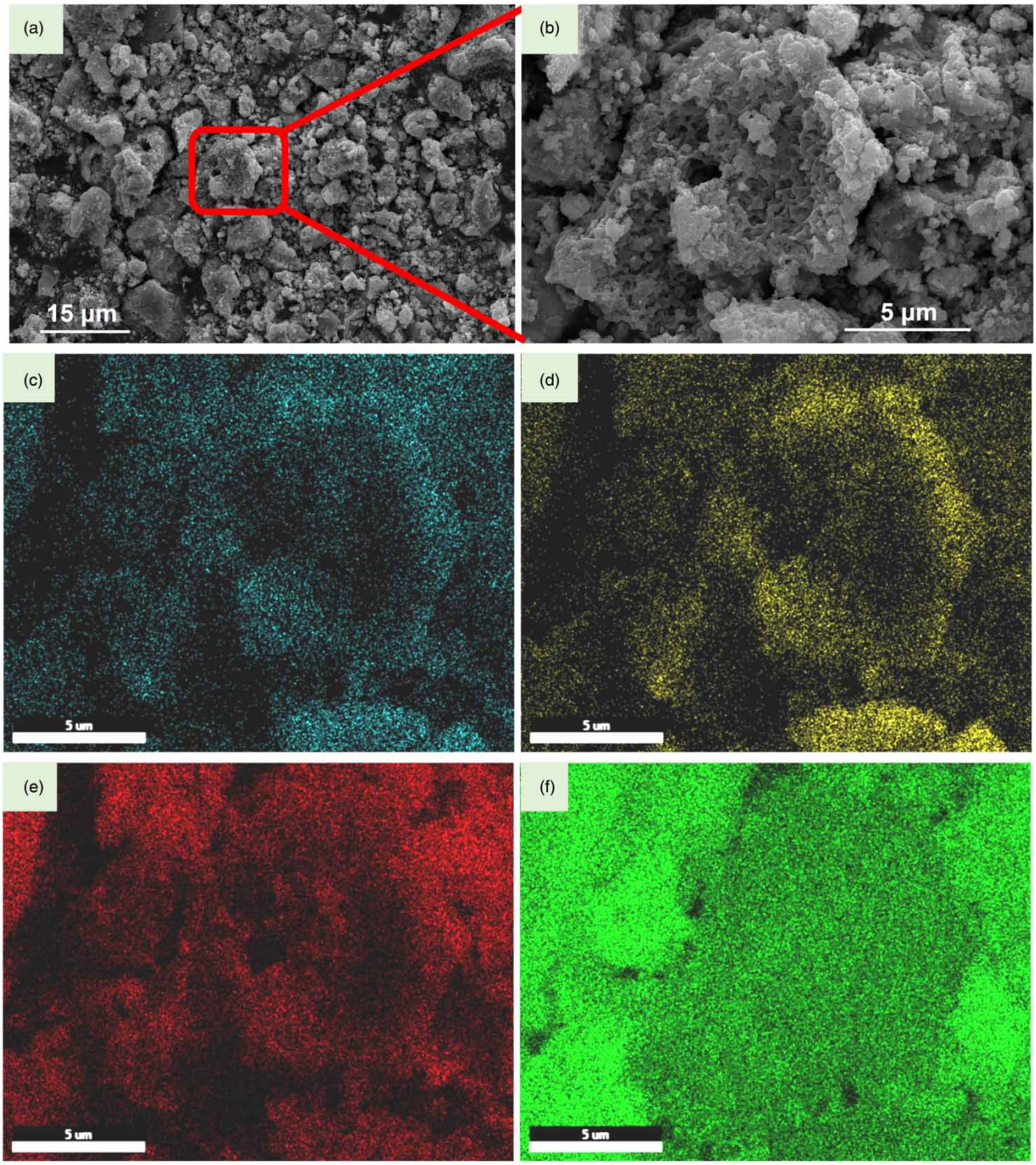

Figure 1 | (a) and (b) Micro-morphology of Cu-C_3N_4, and elemental distribution: (c) C, (d) N, (e) O, and (f) Cu.

first-order model has been extensively reported for studying the kinetics of Fenton-like processes (Wang *et al.* 2021b). Linear fitting of the model offers the apparent rate constant of pseudo first-order kinetics. The rate constant is significantly improved from 0.019 to 0.048 min^{-1} with the assistance of ultrasound (Fig. S5). The catalytic system of Cu-C_3N_4/H_2O_2/ultrasound was used for subsequent degradation experiments.

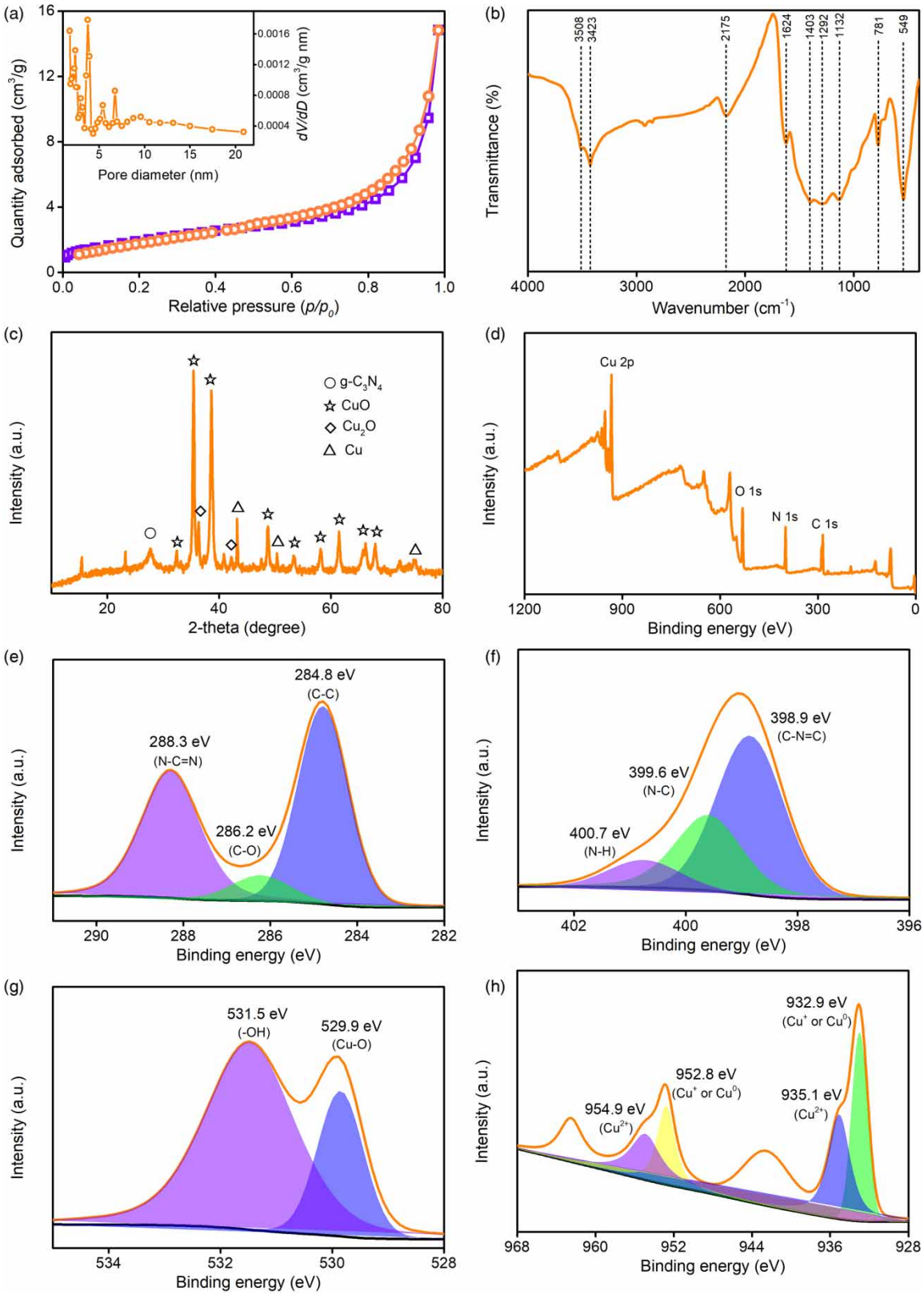

Figure 2 | (a) N_2 adsorption–desorption isotherm, (b) FTIR spectrum, (c) XRD pattern, (d) full XPS spectra, (e) high-resolution C 1s spectra, (f) high-resolution N 1s spectra, (g) high-resolution O 1s spectra, and (h) high-resolution Cu 2p spectra of Cu-C_3N_4.

The proper dosage of catalyst needs to be determined since it is closely related to operation cost for application. Figure 3(a) shows MB removal in the presence of different Cu-C_3N_4 dosage. MB removal is notably improved when increasing Cu-C_3N_4 from 0 to 0.1 g/L. When Cu-C_3N_4 is increased from 0.1 to 0.4 g/L, the removal is slightly enhanced. MB removal is nearly unchanged with further increasing Cu-C_3N_4 dosage. The apparent rate constant is 0.004 min^{-1}, 0.029 min^{-1}, 0.042 min^{-1}, 0.081 min^{-1}, and 0.087 min^{-1}, respectively (Figure 3(b)). The improved MB degradation associated with catalyst dosage was reported by Qin *et al.* (2018). The improvement of MB removal with increasing Cu-C_3N_4 is due to introducing more active sites, benefiting the generation of radical species that promote the degradation reactions (Wang *et al.* 2021b). MB removal is not further enhanced with excessive catalyst, probably because of particle agglomeration of the catalyst and undesirable scavenging radicals (Qin *et al.* 2018). 0.4 g/L of Cu-C_3N_4 was selected as optimal dosage for MB removal.

Effect of H_2O_2 concentration

Figure 4(a) displays MB removal in the presence of different H_2O_2 concentration. MB removal is ineffective in the absence of H_2O_2 (Fig. S6), implying the poor adsorption ability of Cu-C_3N_4 and minor effect of ultrasound (Wang *et al.* 2020a, 2021b). MB removal is sharply promoted in the presence of 10 mM H_2O_2. The removal is further improved by adding 20 mM H_2O_2. Further increasing H_2O_2 levels results in slight improvement in MB removal. The effect of H_2O_2 concentration can be verified by the apparent rate constant (Figure 4(b)). Similar results have been reported by Chen *et al.* (2020b) and Xin *et al.* (2021). The positive effect of H_2O_2 is related to the accelerated generation of reactive radicals that are responsible for MB degradation. In the presence of excessive H_2O_2, MB removal is minorly improved. This can be attributed to the undesirable scavenging reactions (Equations (5) and (6)) (Liu *et al.* 2020b; Wang *et al.* 2021b). Additionally, excessive H_2O_2 may cause the self-decomposition into H_2O and O_2 (Equation (7)), and the radical–radical reaction (Equation (8)) causes additional consumption of hydroxyl radical (Yuan *et al.* 2019; Wang *et al.* 2020b). 20 mM of H_2O_2 was selected for MB removal:

$$H_2O_2 + \bullet OH \rightarrow \bullet OOH + H_2O \quad (5)$$

$$\bullet OOH + \bullet OH \rightarrow O_2 + H_2O \quad (6)$$

$$2H_2O \rightarrow O_2 + 2H_2O \quad (7)$$

$$\bullet OH + \bullet OH \rightarrow H_2O_2 \quad (8)$$

Effect of solution pH

Solution pH is a key parameter for the Fenton-like process, and it influences the oxidation potential of reactive radicals, the stability of H_2O_2, and the reactivity of catalysts (Sun *et al.* 2021). The effect of solution pH on MB removal is shown in Figure 5(a). MB degradation remains almost the same over broad pH regions of 3.3–9.9. Although there exists a small difference in the apparent rate constant (Figure 5(b)), effective MB removal is achieved within 40 min under different pH value. This can be ascribed to the wide operation pH of copper ion. Generally, iron-based catalysts suffer from the narrow operation

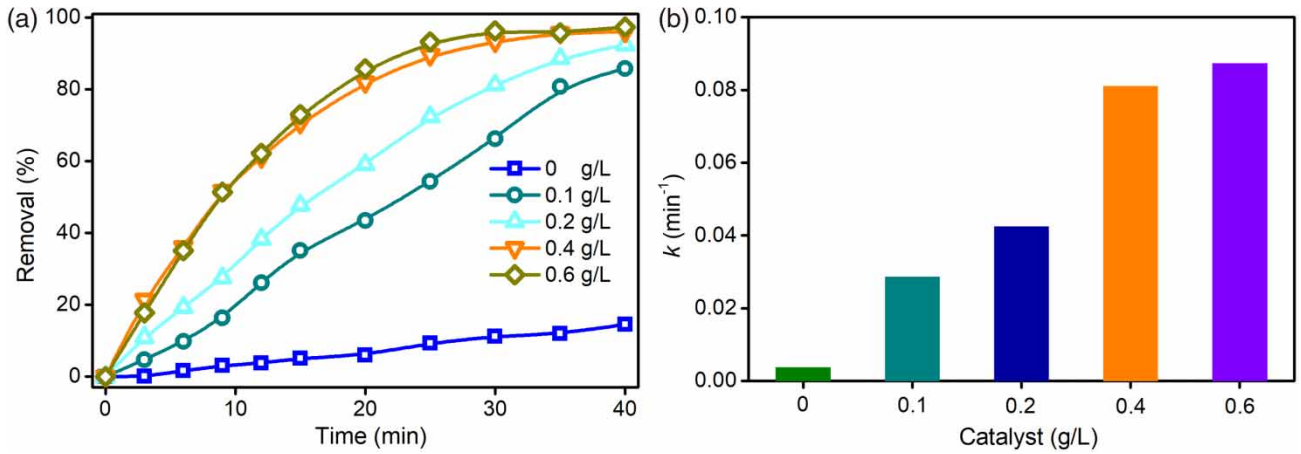

Figure 3 | (a) Effect of Cu-C_3N_4 dosage on MB removal, (b) the apparent rate constant. (Experimental conditions: H_2O_2 20 mM, solution pH 6.7, MB 10 mg/L, and ultrasound.)

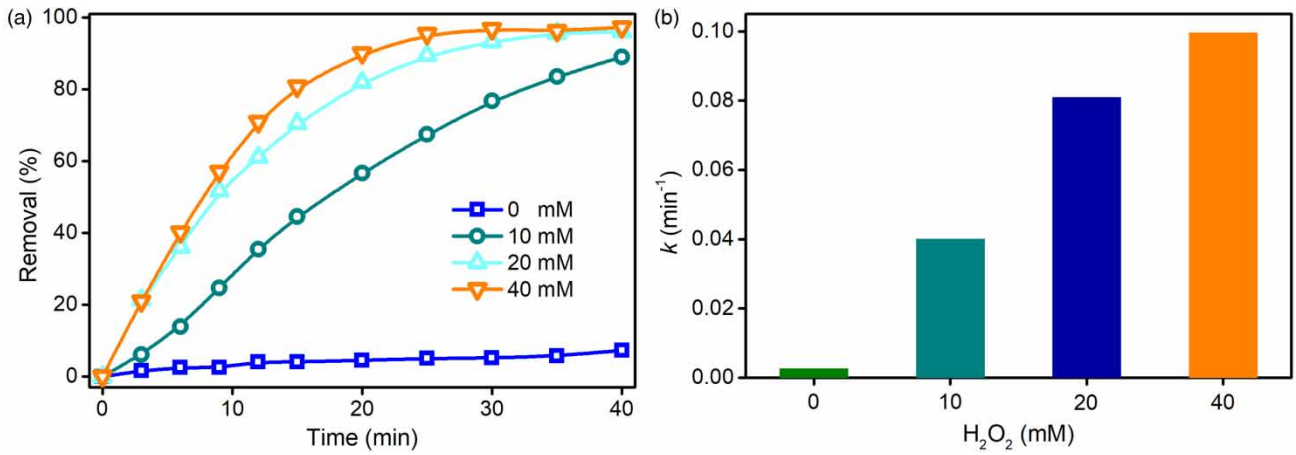

Figure 4 | (a) Effect of H_2O_2 concentration on MB removal, (b) the apparent rate constant. (Experimental conditions: Cu-C_3N_4 0.4 g/L, solution pH 6.7, MB 10 mg/L, and ultrasound.)

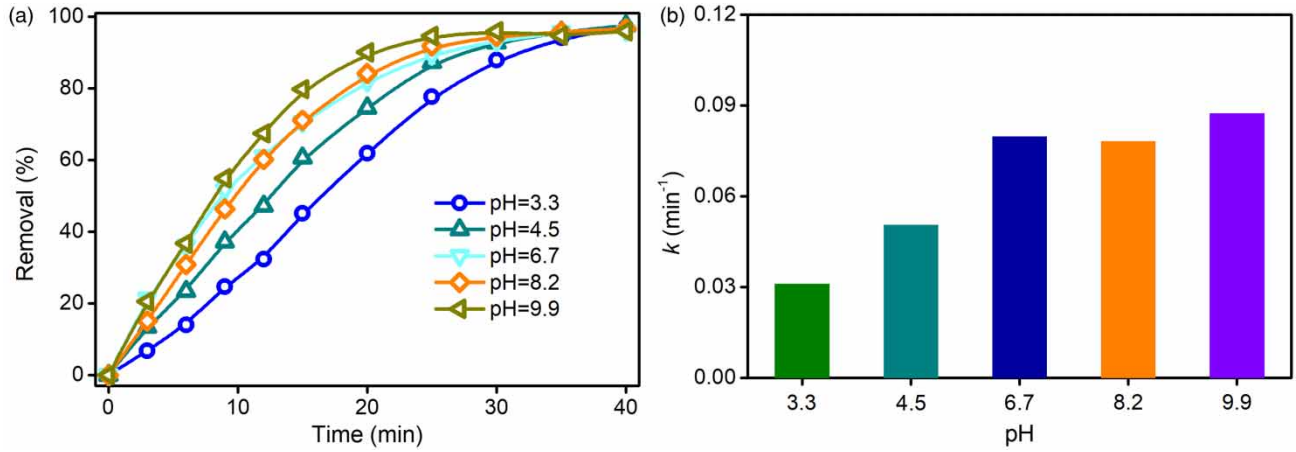

Figure 5 | (a) Effect of solution pH on MB removal, (b) the apparent rate constant. (Experimental conditions: Cu-C_3N_4 0.4 g/L, H_2O_2 20 mM, MB 10 mg/L, and ultrasound.)

pH (Yin *et al.* 2020; de Melo Costa-Serge *et al.* 2021). Dye degradation at neutral pH has been highlighted by many researchers (Šuligoj *et al.* 2020; Wang *et al.* 2020b). Effective MB degradation obtained in a broad pH range is superior to the conventional Fenton process and iron-based catalysts.

Effect of MB concentration

The dye concentration in real wastewater varies with time and sources, and thus it is required to evaluate the effect of initial dye concentration. Figure 6(a) displays MB degradation with different initial MB concentration. MB removal increases with increasing reaction time. Effective degradation of MB solution with higher concentration can be obtained by extending reaction time, suggesting the feasibility of MB removal with different concentration. As observed in Figure 6(b), the apparent rate constant is reduced from 0.0810 to 0.0225 min^{-1} when the initial MB concentration increases from 10 to 30 mg/L. The removal is decreased with an increase in MB concentration. This can be ascribed to the lack of enough reactive radicals (Wang *et al.* 2020b). Additionally, high MB concentration generates more degradation intermediates, which potentially poison catalyst surface (Wang *et al.* 2019c).

Reusability of catalyst

To evaluate the practicability of real application, the reusability of Cu-C_3N_4 was determined in the catalytic system. MB removal is slightly decreased (approximate 7%) for four runs (Figure 7). Obvious decline in MB removal is seen for fifth

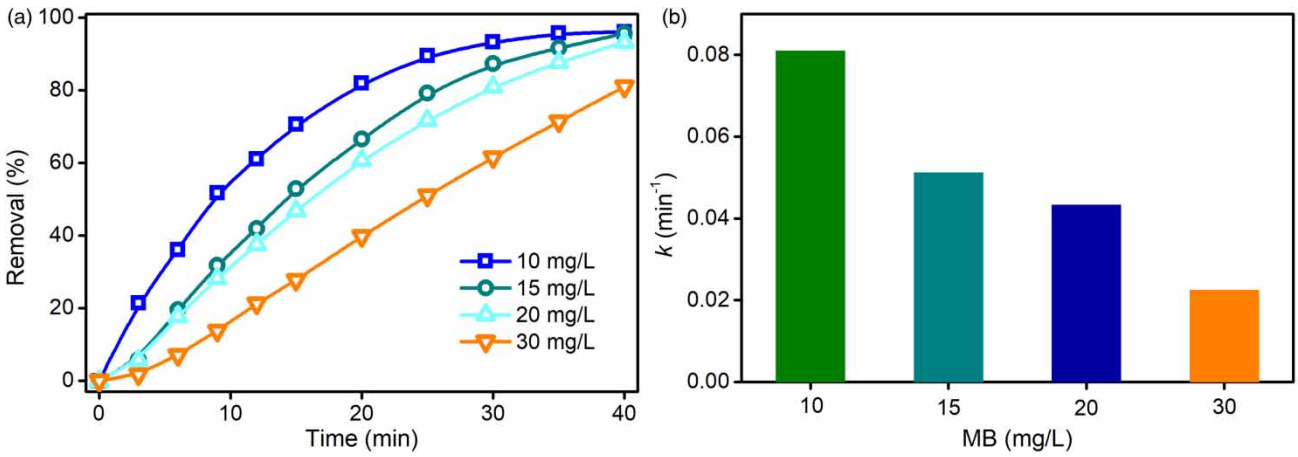

Figure 6 | (a) Effect of initial MB concentration on MB removal, (b) the apparent rate constant. (Experimental conditions: Cu-C_3N_4 0.4 g/L, H_2O_2 20 mM, solution pH 6.7, and ultrasound.)

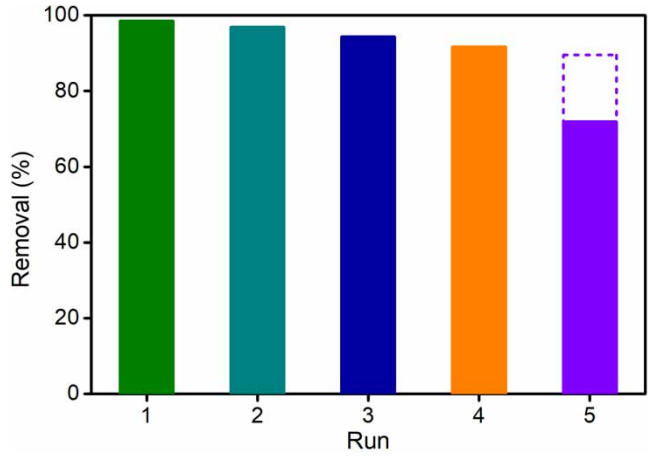

Figure 7 | The reusability of catalyst in Cu-C_3N_4/H_2O_2/ultrasound system. (Experimental conditions: Cu-C_3N_4 0.4 g/L, H_2O_2 20 mM, solution pH 6.7, MB 10 mg/L, and ultrasound.)

run, but effective MB removal can be obtained by prolonging reaction time (60 min). The results suggest the good reusability for application. Cu-C_3N_4 as Fenton-like catalyst has outstanding advantages such as high activity, broad operation pH, and good reusability. The process is promising for potential application to wastewater treatment.

Mechanism of catalytic reactions

Figure 8(a) displays the UV–vis spectra of MB solution. The peak at 664 nm is assigned to the chromophore groups (C = S and C = N bonds) in MB molecules (Fig. S7) (Wang *et al.* 2020b). The rapid decrease of the peak at 664 nm is observed with slight shift. This indicates that MB degradation is predominated by chromophore cleavage in the early stage under experimental conditions (He *et al.* 2009). The hypsochromic shift of the characteristic peak at later stage suggests the possible pathway of N-de-ethylation due to the auxochromic property of the N-ethyl group (Mitoraj *et al.* 2018). The degradation intermediates may undergo other reactions including hydroxylation, aromatic ring opening and mineralization (Zhou *et al.* 2015). MB degradation can be verified by the color change of MB solution (Fig. S8). The dark blue color becomes gradually colorless, and complete discoloration is achieved within 40 min. The color change of MB solution is consistent to the time-dependent UV–vis spectra.

MB removal in the presence of Cu-C_3N_4 is negligible within 120 min. The result implies the minor role of adsorption in MB removal, probably due to the small surface area of Cu-C_3N_4. Fenton-like reactions play dominated role in MB removal.

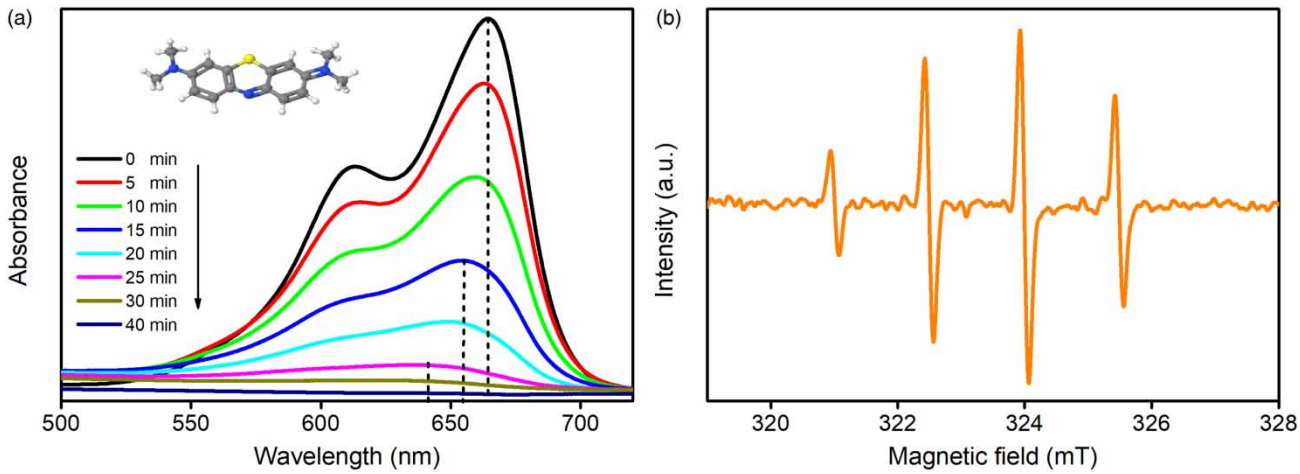

Figure 8 | (a) UV–vis spectra of MB solution associated with different reaction time, (b) ESR spectrum of DMPO-trapped •OH.

Copper species in Cu-C_3N_4 provide active sites to activate H_2O_2 for the generation of reactive radicals (Liu *et al.* 2021). Cu^0 can be converted into Cu^+ (Equation (9)). Cu^+ reacts with H_2O_2 to generate •OH. Cu^{2+} can be reduced to Cu^+ by reaction with H_2O_2, realizing the Cu^{2+}/Cu^+ cycle. In the catalytic system, more radical species are generated assisted by ultrasound. Ultrasound also enables H_2O_2 activation into •OH radicals (Equations (10)–(12)) (Prakash *et al.* 2020; Wang *et al.* 2020a):

$$2Cu^0 + H_2O_2 \rightarrow 2Cu^+ + 2HO^- \quad (9)$$

$$H_2O +))) \rightarrow \bullet OH + \bullet H \quad (10)$$

$$H_2O_2 +))) \rightarrow 2\bullet OH \quad (11)$$

$$Cu^+ +))) \rightarrow Cu^{2+} + e^- \quad (12)$$

The radicals are responsible for MB degradation. As reported by previous studies, •OH is the dominant oxidant in Fenton-like processes (Wang *et al.* 2019a; Xin *et al.* 2021). To verify the role of •OH in the Cu-C_3N_4/H_2O_2/ultrasound system, IPA is used as radical scavenger. Fig. S9 displays MB removal, which is lowered in the presence of IPA, and which is attributed to the scavenging effect. The existence of •OH is further confirmed by ESR spectrum using DMPO as a probe. A strong 4-fold characteristic peak of typical DMPO-trapped •OH adduct with an intensity ratio of 1:2:2:1 is observed in Figure 8(b) (Xin *et al.* 2021). It should be noted that besides •OH, other radicals cannot be ruled out for MB degradation. Based on above analysis, the plausible catalytic mechanism in Cu-C_3N_4/H_2O_2/ultrasound system is schematically shown in Figure 9.

Degradation of different dyes including azo dye (AO7) and triphenylmethane dye (RhB) were further conducted. Figure 10(a) manifests the UV–vis spectra of RhB. The maximum peak at 554 nm is ascribed to the N-ethyl group of RhB (Wang *et al.* 2021b). Effective degradation of RhB is obtained within 30 min as verified by the sharp decline of peak at 554 nm. The pathway of RhB degradation involves chromophore groups and N-de-ethylation (Wang *et al.* 2020a). Similar to MB degradation, the degradation of RhB is dominated by chromophore cleavage, while N-de-ethylation succeeded. Figure 10(b) shows that the typical peak at 484 nm of AO7 significantly declined within 40 min, validating the effective degradation of AO7 in the catalytic system (Wang *et al.* 2019c). Unlike MB degradation, obvious shift of the characteristic peak occurs in the initial stage, suggesting that degradation is not controlled by chromophore cleavage. The results verify that different dyes can be effectively degraded in the Cu-C_3N_4/H_2O_2/ultrasound system.

CONCLUSIONS

As verified by SEM, XRD, FTIR, and XPS, Cu-C_3N_4 contains copper species of Cu, Cu_2O and CuO, which are uniformly doped on the surface of porous g-C_3N_4. Enhanced MB degradation is observed by ultrasound. MB degradation in the Cu-C_3N_4/H_2O_2/ultrasound system is described by pseudo first-order kinetics. MB degradation is influenced by catalyst dosage, H_2O_2 concentration, solution pH, and initial MB concentration. Under conditions of Cu-C_3N_4 0.4 g/L, H_2O_2

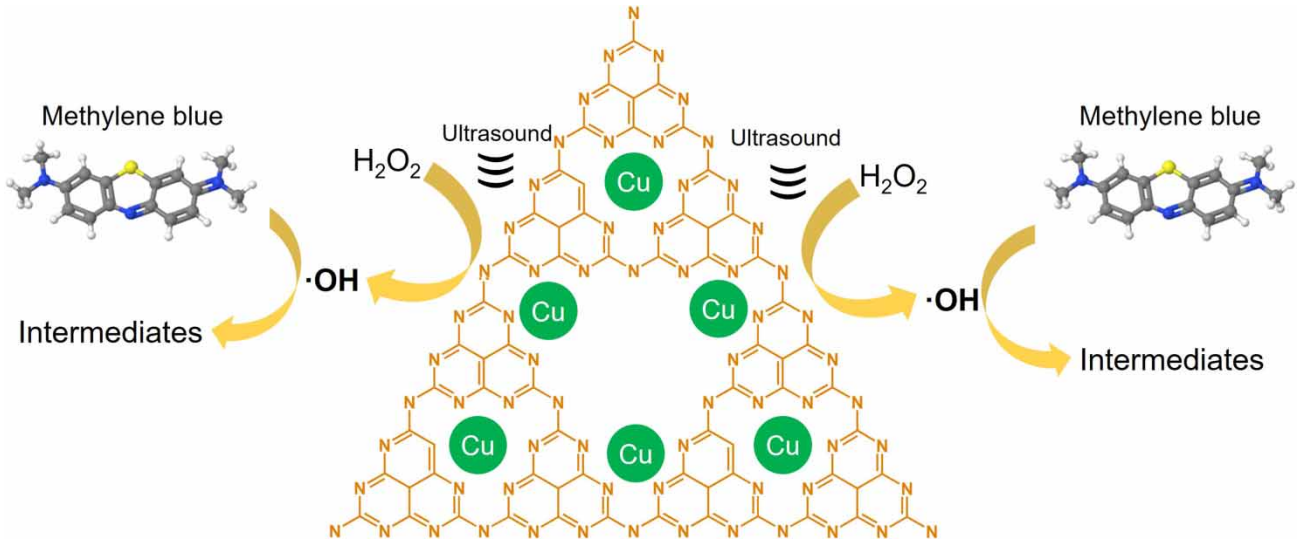

Figure 9 | Schematical scheme of plausible catalytic mechanism in Cu-C_3N_4/H_2O_2/ultrasound system.

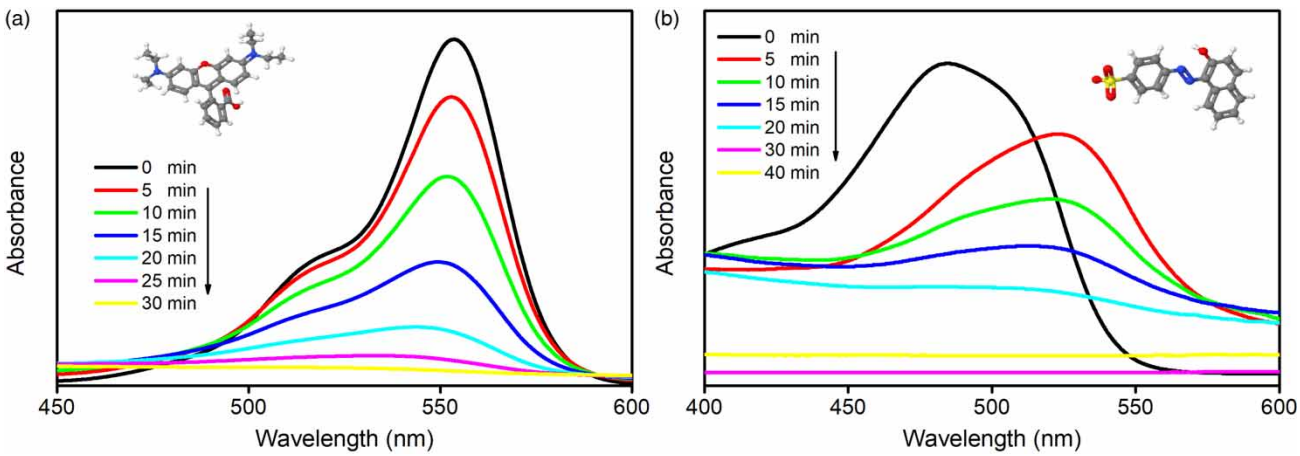

Figure 10 | Time-dependent UV–vis spectra of (a) RhB and (b) AO7 solution.

20 mM, solution pH 6.7, MB 10 mg/L, and ultrasound, MB degradation of 96% is obtained within 30 min, and the corresponding rate constant is 0.099 min^{-1}. Effective MB degradation over a broad pH range (3.3–9.9) is superior to the conventional Fenton process or iron-based catalysts. Cu-C_3N_4 has good reusability as Fenton-like catalysts. Quenching test and ESR spectrum confirmed the existence of •OH in the catalytic system. Ultrasonically improved H_2O_2 activation by Cu-C_3N_4 for the generation of •OH radical is the dominant mechanism for MB degradation. The degradation of RhB and AO7 is also effectively achieved. The commercial application of the catalytic system for wastewater treatment requires more efforts. Nevertheless, this work provides insights into designing Fenton-like catalysts and wastewater treatment.

ACKNOWLEDGEMENTS

This work was supported by the National Natural Science Foundation of China (51804276); and the Excellent Youth Scientist of China Association for Science and Technology.

COMPETING INTERESTS STATEMENT

The authors have no competing interests to declare.

DATA AVAILABILITY STATEMENT

Data cannot be made publicly available; readers should contact the corresponding author for details.

REFERENCES

Bokare, A. D. & Choi, W. 2014 Review of iron-free Fenton-like systems for activating H_2O_2 in advanced oxidation processes. *Journal of Hazardous Materials* **275**, 121–135.

Chanikya, P., Nidheesh, P. V., Babu, D. S., Gopinath, A. & Kumar, M. S. 2021 Treatment of dyeing wastewater by combined sulfate radical based electrochemical advanced oxidation and electrocoagulation processes. *Separation and Purification Technology* **254**, 117570.

Chen, Z., Zhang, S., Liu, Y., Alharbi, N. S., Rabah, S. O., Wang, S. & Wang, X. 2020a Synthesis and fabrication of g-C_3N_4-based materials and their application in elimination of pollutants. *Science of the Total Environment* **731**, 139054.

Chen, X. L., Li, F., Chen, H., Wang, H. & Li, G. 2020b Fe_2O_3/TiO_2 functionalized biochar as a heterogeneous catalyst for dyes degradation in water under Fenton processes. *Journal of Environmental Chemical Engineering* **8** (4), 103905.

de Melo Costa-Serge, N., Gonçalves, R. G. L., Rojas-Mantilla, H. D., Santilli, C. V., Hammer, P. & Nogueira, R. F. P. 2021 Fenton-like degradation of sulfathiazole using copper-modified MgFe-CO_3 layered double hydroxide. *Journal of Hazardous Materials* **413**, 125388.

Dong, Q., Chen, Y., Wang, L., Ai, S. & Ding, H. 2017 Cu-modified alkalinized g-C_3N_4 as photocatalytically assisted heterogeneous Fenton-like catalyst. *Applied Surface Science* **426**, 1133–1140.

Feng, L., Wang, R., Zhang, Y., Ji, S., Chuan, Y., Zhang, W. & Du, C. 2019 In situ XRD observation of CuO anode phase conversion in lithium-ion batteries. *Journal of Materials Science* **54** (2), 1520–1528.

Gawande, M. B., Goswami, A., Felpin, F. X., Asefa, T., Huang, X., Silva, R. & Varma, R. S. 2016 Cu and Cu-based nanoparticles: synthesis and applications in catalysis. *Chemical Reviews* **116** (6), 3722–3811.

Hasija, V., Nguyen, V. H., Kumar, A., Raizada, P., Krishnan, V., Khan, A. A. P. & Huong, P. T. 2021 Advanced activation of persulfate by polymeric g-C_3N_4 based photocatalysts for environmental remediation: a review. *Journal of Hazardous Materials* **413**, 125324.

He, Z., Sun, C., Yang, S., Ding, Y., He, H. & Wang, Z. 2009 Photocatalytic degradation of rhodamine B by Bi_2WO_6 with electron accepting agent under microwave irradiation: mechanism and pathway. *Journal of Hazardous Materials* **162** (2–3), 1477–1486.

Hu, J., Zhang, P., An, W., Liu, L., Liang, Y. & Cui, W. 2019a In-situ Fe-doped g-C_3N_4 heterogeneous catalyst via photocatalysis-Fenton reaction with enriched photocatalytic performance for removal of complex wastewater. *Applied Catalysis B: Environmental* **245**, 130–142.

Jiang, Y., Xie, Q., Zhang, Y., Geng, C., Yu, B. & Chi, J. 2019 Preparation of magnetically separable mesoporous activated carbons from brown coal with Fe_3O_4. *International Journal of Mining Science and Technology* **29** (3), 513–519.

Jourshabani, M., Lee, B. K. & Shariatinia, Z. 2020 From traditional strategies to Z-scheme configuration in graphitic carbon nitride photocatalysts: recent progress and future challenges. *Applied Catalysis B: Environmental* **276**, 119157.

Kothai, A., Sathishkumar, C., Muthupriya, R. & Dharchana, R. 2021 Experimental investigation of textile dyeing wastewater treatment using aluminium in electro coagulation process and Fenton's reagent in advanced oxidation process. *Materials Today: Proceedings* **45**, 1411–1416.

Kumar, S., Baruah, A., Tonda, S., Kumar, B., Shanker, V. & Sreedhar, B. 2014 Cost-effective and eco-friendly synthesis of novel and stable N-doped ZnO/gC_3N_4 core–shell nanoplates with excellent visible-light responsive photocatalysis. *Nanoscale* **6** (9), 4830–4842.

Li, X., Huang, X., Xi, S., Miao, S., Ding, J., Cai, W., Liu, S., Yang, X., Yang, H., Gao, J., Wang, J., Huang, Y. & Liu, B. 2018a Single cobalt atoms anchored on porous N-doped graphene with dual reaction sites for efficient Fenton-like catalysis. *Journal of the American Chemical Society* **140** (39), 12469–12475.

Liu, P. & Hensen, E. J. 2013 Highly efficient and robust Au/$MgCuCr_2O_4$ catalyst for gas-phase oxidation of ethanol to acetaldehyde. *Journal of the American Chemical Society* **135** (38), 14032–14035.

Liu, X., Ma, R., Zhuang, L., Hu, B., Chen, J., Liu, X. & Wang, X. 2020b Recent developments of doped g-C_3N_4 photocatalysts for the degradation of organic pollutants. *Critical Reviews in Environmental Science and Technology* **51** (8), 1–40.

Liu, Y., Yang, Z. & Wang, J. 2021 Fenton-like degradation of sulfamethoxazole in Cu^0/Zn^0-air system over a broad pH range: performance, kinetics and mechanism. *Chemical Engineering Journal* **403**, 126320.

Ma, J., Yang, Q., Wen, Y. & Liu, W. 2017 Fe-g-C_3N_4/graphitized mesoporous carbon composite as an effective Fenton-like catalyst in a wide pH range. *Applied Catalysis B: Environmental* **201**, 232–240.

Mian, M. & Liu, G. 2018 Recent progress in biochar-supported photocatalysts: synthesis, role of biochar, and applications. *RSC Advances* **8** (26), 14237–14248.

Mitoraj, D., Lamdab, U., Kangwansupamonkon, W., Pacia, M., Macyk, W., Wetchakun, N. & Beranek, R. 2018 Revisiting the problem of using methylene blue as a model pollutant in photocatalysis: the case of $InVO_4$/$BiVO_4$ composites. *Journal of Photochemistry and Photobiology A: Chemistry* **366**, 103–110.

Muniandy, L., Adam, F., Mohamed, A. R., Iqbal, A. & Rahman, N. R. A. 2017 Cu^{2+} coordinated graphitic carbon nitride (Cu-g-C_3N_4) nanosheets from melamine for the liquid phase hydroxylation of benzene and VOCs. *Applied Surface Science* **398**, 43–55.

Nguyen, T. K. A., Pham, T. T., Nguyen-Phu, H. & Shin, E. W. 2021 The effect of graphitic carbon nitride precursors on the photocatalytic dye degradation of water-dispersible graphitic carbon nitride photocatalysts. *Applied Surface Science* **537**, 148027.

Omrani, N. & Nezamzadeh-Ejhieh, A. 2020 Focus on scavengers' effects and GC-MASS analysis of photodegradation intermediates of sulfasalazine by Cu_2O/CdS nanocomposite. *Separation and Purification Technology* **235**, 116228.

Prakash, L. V., Gopinath, A., Gandhimathi, R., Velmathi, S., Ramesh, S. T. & Nidheesh, P. V. 2020 Ultrasound aided heterogeneous Fenton degradation of Acid Blue 15 over green synthesized magnetite nanoparticles. *Separation and Purification Technology* **266**, 118230.

Qin, Q., Liu, Y., Li, X., Sun, T. & Xu, Y. 2018 Enhanced heterogeneous Fenton-like degradation of methylene blue by reduced CuFe 2 O 4. *RSC Advances* **8** (2), 1071–1077.

Qin, Z., Chang, P., Ma, L., Bu, L. & Song, Z. 2019 Preparation and modulation of a novel thin-walled carbon foam. *International Journal of Mining Science and Technology* **29** (2), 281–287.

Routoula, E. & Patwardhan, S. V. 2020 Degradation of anthraquinone dyes from effluents: a review focusing on enzymatic dye degradation with industrial potential. *Environmental Science & Technology* **54** (2), 647–664.

Shah, N. S., Khan, J. A., Sayed, M., Iqbal, J., Khan, Z. U. H., Muhammad, N. & Nazzal, Y. 2020 Nano-zerovalent copper as a Fenton-like catalyst for the degradation of ciprofloxacin in aqueous solution. *Journal of Water Process Engineering* **37**, 101325.

Song, H., Guan, Z., Xia, D., Xu, H., Yang, F., Li, D. & Li, X. 2021 Copper-oxygen synergistic electronic reconstruction on g-C_3N_4 for efficient non-radical catalysis for peroxydisulfate and peroxymonosulfate. *Separation and Purification Technology* **257**, 117957.

Sun, R., Zhang, X., Wang, C. & Cao, Y. 2021 Co-carbonization of red mud and waste sawdust for functional application as Fenton catalyst: evaluation of catalytic activity and mechanism. *Journal of Environmental Chemical Engineering* **9** (4), 105368.

Šuligoj, A., Ristić, A., Dražić, G., Pintar, A., Logar, N. Z. & Tušar, N. N. 2020 Bimetal Cu-Mn porous silica-supported catalyst for Fenton-like degradation of organic dyes in wastewater at neutral pH. *Catalysis Today* **358**, 270–277.

Wang, C., Cao, Y. & Wang, H. 2019a Copper-based catalyst from waste printed circuit boards for effective Fenton-like discoloration of Rhodamine B at neutral pH. *Chemosphere* **230**, 278–285.

Wang, L., Zhu, Y., Yang, D., Zhao, L., Ding, H. & Wang, Z. 2019b The mixed marriage of copper and carbon ring-g-C_3N_4 nanosheet: a visible-light-driven heterogeneous Fenton-like catalyst. *Applied Surface Science* **488**, 728–738.

Wang, C., Wang, H. & Cao, Y. 2019c Waste printed circuit boards as novel potential engineered catalyst for catalytic degradation of orange II. *Journal of Cleaner Production* **221**, 234–241.

Wang, C., Wang, H. & Cao, Y. 2020a Ultrasonic improvement of catalytic decomposition of Rhodamine B in simulated wastewater by functional waste printed circuit boards via thermochemical conversion. *Journal of Cleaner Production* **253**, 119921.

Wang, C., Huang, R. & Sun, R. 2020b Green one-spot synthesis of hydrochar supported zero-valent iron for heterogeneous Fenton-like discoloration of dyes at neutral pH. *Journal of Molecular Liquids* **320**, 114421.

Wang, C., Sun, R., Huang, R. & Wang, H. 2021a Superior Fenton-like degradation of tetracycline by iron loaded graphite carbon derived from microplastics: synthesis, catalytic performance, and mechanism. *Separation and Purification Technology* **270**, 118773.

Wang, C., Sun, R. & Huang, R. 2021b Highly dispersed iron-doped biochar derived from sawdust for Fenton-like degradation of toxic dyes. *Journal of Cleaner Production* **297**, 126681.

Wu, Q., Wang, J., Wang, Z., Xu, Y., Xing, Z., Zhang, X. & Li, X. 2020 High-loaded single Cu atoms decorated on N-doped graphene for boosting Fenton-like catalysis under neutral pH. *Journal of Materials Chemistry A* **8** (27), 13685–13693.

Xin, S., Liu, G., Ma, X., Gong, J., Ma, B., Yan, Q. & Xin, Y. 2021 High efficiency heterogeneous Fenton-like catalyst biochar modified $CuFeO_2$ for the degradation of tetracycline: economical synthesis, catalytic performance and mechanism. *Applied Catalysis B: Environmental* **280**, 119386.

Yang, Y., Li, X., Zhou, C., Xiong, W., Zeng, G., Huang, D. & Guo, H. 2020 Recent advances in application of graphitic carbon nitride-based catalysts for degrading organic contaminants in water through advanced oxidation processes beyond photocatalysis: a critical review. *Water Research* **184**, 116200.

Yao, Y., Lu, F., Zhu, Y., Wei, F., Liu, X., Lian, C. & Wang, S. 2015 Magnetic core–shell $CuFe_2O_4$@C_3N_4 hybrids for visible light photocatalysis of Orange II. *Journal of Hazardous Materials* **297**, 224–233.

Yin, Y., Li, W., Xu, C., Shi, L., Zhang, L. C., Ao, Z., Liu, M., Lu, M., Duan, X., Wang, S., Liu, S. & Sun, H. 2020 Ultrafine copper nanoclusters and single sites for Fenton-like reactions with high atom utilities. *Environmental Science: Nano* **7** (9), 2595–2606.

Yuan, D., Zhang, C., Tang, S., Li, X., Tang, J., Rao, Y. & Zhang, Q. 2019 Enhancing CaO_2 Fenton-like process by Fe (II)-oxalic acid complexation for organic wastewater treatment. *Water Research* **163**, 114861.

Zhang, L., Xu, D., Hu, C. & Shi, Y. 2017 Framework Cu-doped $AlPO_4$ as an effective Fenton-like catalyst for bisphenol A degradation. *Applied Catalysis B: Environmental* **207**, 9–16.

Zhang, J., Yuan, M., Liu, X., Wang, X., Liu, S., Han, B. & Shi, H. 2020a Copper modified Ti^{3+} self-doped TiO_2 photocatalyst for highly efficient photodisinfection of five agricultural pathogenic fungus. *Chemical Engineering Journal* **387**, 124171.

Zhang, Y., Jiang, H., Wang, H. & Wang, C. 2020b Separation of hazardous polyvinyl chloride from waste plastics by flotation assisted with surface modification of ammonium persulfate: process and mechanism. *Journal of Hazardous Materials* **389**, 121918.

Zhou, G., Fang, F., Chen, Z., He, Y., Sun, H. & Shi, H. 2015 Facile synthesis of paper mill sludge-derived heterogeneous catalyst for the Fenton-like degradation of methylene blue. *Catalysis Communications* **62**, 71–74.

Zhu, J. N., Zhu, X. Q., Cheng, F. F., Li, P., Wang, F., Xiao, Y. W. & Xiong, W. W. 2019 Preparing copper doped carbon nitride from melamine templated crystalline copper chloride for Fenton-like catalysis. *Applied Catalysis B: Environmental* **256**, 117830.

First received 14 April 2021; accepted in revised form 8 July 2021. Available online 19 July 2021